Theory of Time-Dependent Multiple Backscattering from Clouds

QIMING CAI[1] AND KUO-NAN LIOU

Department of Meteorology, University of Utah, Salt Lake City 84112

(Manuscript received 17 November 1980, in final form 16 March 1981)

ABSTRACT

Time-dependent transfer models for double, triple and general multiple backscattering problems involving the integration of a pulsed laser beam and clouds have been developed using a spherical polar coordinate system. The general solution of the time-dependent multiple-backscattering problem is expressed in terms of a series of integral equations based on specific geometrical considerations under the time constraint of the return pulses. The theory developed includes a general four-by-four scattering phase matrix and requires no specific physical approximations. Numerical computations have been carried out for doubly and triply backscattered powers employing the phase matrix for a typical cumulus cloud composed exclusively of water droplets illuminated by laser wavelengths of 0.7 and 10.6 μm. We investigate effects of the transmitter beam width and receiver field-of-view on the multiply backscattered return, and depolarization and polarization characteristics. We also examine comprehensively and discuss physically the relative contributions due to primary, double and triple backscattering as functions of the laser penetration depth. Highlights and new finds derived from this theoretical analysis are presented and finally summarized in the conclusion.

1. Introduction

In recent years, a lidar backscattering technique has been developed for the discrimination between water and ice clouds based on the single-scattering principle that spherical water droplets will retain the polarization characteristic of the incident energy, whereas ice crystals will generate a significant amount of depolarization caused by the nonsphericity of hexagonal and irregular structures. The fundamental difficulty in the interpretation of the data associated with this technique and all other lidar cloud-sounding techniques utilizing a pulsed laser system has been the effect of multiple scattering. Although significant progress has been made in time-dependent multiple-backscattering analyses (Liou, 1971; Liou and Schotland, 1971; Weinman, 1976), the definitive and quantitative assessment of multiple-scattering effects in the lidar backscattering experiment is still an area requiring further investigation.

Moreover, results of field observations (Pal and Carswell, 1973; Houston and Carswell, 1978) and laboratory experiments (Sassen and Liou, 1979a,b) have illustrated convincingly the significance of the polarization information content, in addition to the flux component, with respect to the sounding of the cloud compositions and structure. Therefore, it appears to be theoretically important and practically desirable to investigate from an analytical point of view the complete information content of the backscattered Stokes parameters in relation to the development of cloud-sounding techniques.

Bearing in mind the uncertainty of the multiple-scattering effect in backscattering interpretations and the probable information content of the backscattered polarization for the inference of cloud compositions and structure, we have developed in this paper a theoretical model for time-dependent multiple backscattering involving clouds, which for the first time includes a general four-by-four scattering phase matrix. The theoretical development is general and requires no specific physical approximations in the mathematical formulation. Sections 2, 3 and 4 contain analytical formulations of double, triple and general multiple backscattering, respectively, on the basis of a number of specific geometrical considerations under the time-dependent constraint. In Section 5 computational results for doubly and triply backscattered powers using the scattering phase matrix for a cumulus cloud at wavelengths of 0.7 and 10.6 μm are presented. Effects of the transmitter beamwidth and receiver field-of-view on the backscattered return and polarization characteristics, and relative contributions of primary, double and triple backscattering as functions of the penetration depth are comprehensively studied and physically discussed. Highlights of the computational result are given in Section 6.

[1] On leave from the Lanzhou Institute of Plateau Atmospheric Physics, Academia Sinica, Lanzhou, China.

0022-4928/81/071452-15$07.75

2. Mathematical formulation for double backscattering

Considering a collimated pulsed lidar system in which the transmitter and receiver are coaxial and referring to Fig. 1, we let point O be the origin of the spherical polar coordinate system. The lidar transmits a light pulse to the atmosphere, which is first scattered by cloud particles at point A. A portion of the first scattered light reaches point B at which a secondary scattering event takes place. It follows that a portion of the secondary scattered light pulse returns to point O and is recorded by the receiver. Thus, at a given instant of time the returned energy is the sum of the singly plus multiply backscattered light pulse. We shall first consider only the double backscattering. In order for the singly and doubly backscattered light pulse to reach the receiver at the same given instant of time, there must exist a geometric relationship between R_0, R_1 and R_2 such that (see Fig. 1)

$$\frac{2R_0}{c} = \frac{R_1 + l_1 + R_2}{c}, \tag{1}$$

where R_0 is the distance at which single scattering occurs, R_1 and R_2 the distance between points A and B and point O, respectively, at which primary and double scattering takes place, l_1 the distance between A and B, and c the velocity of light.

If R_1 is considered to be a constant, the time-dependent relationship for double scattering may be written as

$$l_1 + R_2 = 2R_0 - R_1. \tag{2}$$

As shown by Liou (1971), the trace which satisfies Eq. (2) is an ellipse with two foci at points O and A. Based on the geometry, we let $2a$ be the major axis of the ellipse such that

$$2a = l_1 + R_2 = 2R_0 - R_1. \tag{3}$$

We now let the coordinates imposed on points A and B expressed in the spherical polar coordinate system be (ϕ_1, ψ_1, R_1) and (ϕ_2, ψ_2, R_2). The equation of the ellipse with the distance R_1 between two foci and the major axis $2a$ in the spherical polar coordinate system may be written as

$$R_2 = \frac{4a^2 - R_1^2}{4a - 2R_1 \cos\Delta_{21}}, \tag{4}$$

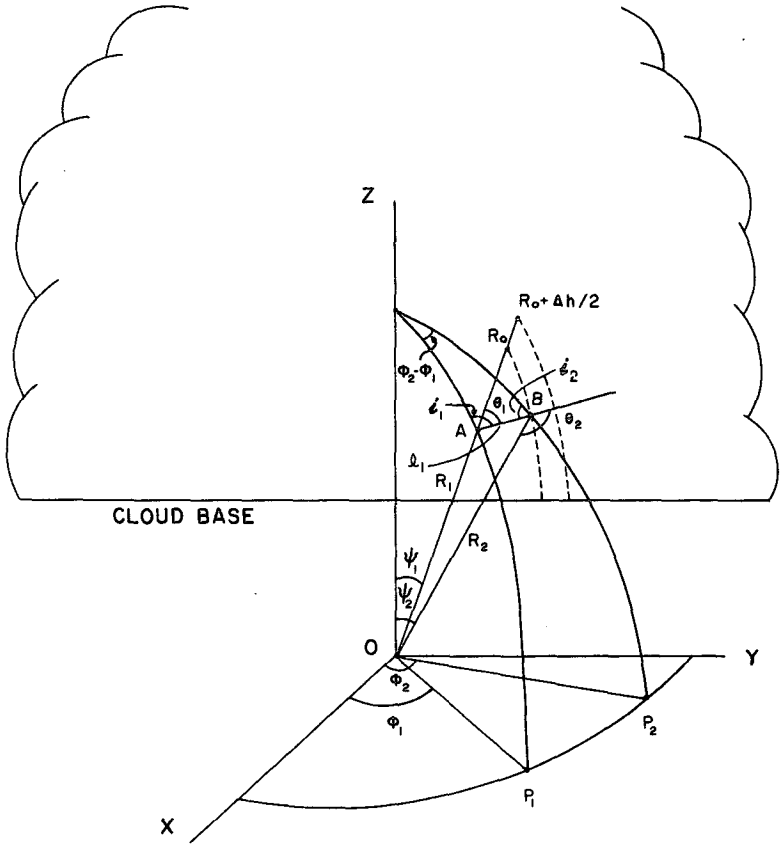

FIG. 1. Geometrical configuration for double backscattering.

where Δ_{21} represents the angle between OA and OB which satisfies the relationship

$$\cos\Delta_{21} = \cos\psi_1 \cos\psi_2 + \sin\psi_1 \sin\psi_2 \times \cos(\phi_2 - \phi_1). \quad (5)$$

Assuming that the light pulse has a geometrical length Δh, then all the doubly backscattered light arriving at the receiver at a given instant of time comes from points within the distance $\Delta h/2$ between two ellipses having the same foci O and A. The inner ellipse is determined by Eq. (4) and the outer ellipse by

$$R_2' = \frac{4a'^2 - R_1^2}{4a' - 2R_1 \cos\Delta_{21}}, \quad (6)$$

$$2a' = 2R_0 - R_1 + \Delta h, \quad (7)$$

where $2a'$ is the major axis of the outer ellipse, and Δh the length of the light pulse. Note that $\Delta h = c\Delta t$ where Δt is the duration of the light pulse.

The foregoing discussions are concerned with the time-dependent scattering geometry as shown in Fig. 1. Now we let dv_1 and dv_2 represent infinitesimal scattering volumes, at the points A and B, respectively. At time $t = 2R_0/c$, the returned flux density due to double backscattering may be expressed by

$$d\mathbf{F}^{(2)} = \frac{\beta_s \mathbf{L}(-i_2)\mathbf{P}(\theta_2) d\mathbf{F}^{(1)} \exp[-\tau(R_2)]}{4\pi R_2^2} dv_2, \quad (8)$$

where $\mathbf{F}^{(2)}$ represents a Stokes vector and is given by four Stokes parameters in the form

$$\mathbf{F} = \begin{bmatrix} F_l \\ F_r \\ U \\ V \end{bmatrix}. \quad (9)$$

In Eq. (8) $d\mathbf{F}^{(1)}$ denotes the incident flux density matrix, scattered at point A with volume dv_1, which reaches point B with volume dv_2, and $\mathbf{P}(\theta_2)$ represents the scattering phase matrix as a function of θ_2 which is the scattering angle for the secondary scattering. Generally, if no assumption has been made, then the phase matrix consists of 16 elements as follows:

$$\mathbf{P}(\theta) = \begin{bmatrix} P_{11} & P_{12} & P_{13} & P_{14} \\ P_{21} & P_{22} & P_{23} & P_{24} \\ P_{31} & P_{32} & P_{33} & P_{34} \\ P_{41} & P_{42} & P_{43} & P_{44} \end{bmatrix}. \quad (10)$$

In addition, β_s (in units of per length) represents the volume scattering cross section defined by

$$\beta_s = \int_{r_1}^{r_2} \sigma_s \frac{dn(r)}{dr} dr, \quad (11)$$

where σ_s is the scattering cross section for a single particle, $dn(r)/dr$ the particle size distribution, and r_1 and r_2 the lower and upper limits of the integration, respectively; $\tau(R_2)$ in Eq. (8) is the optical depth along the path length R_2 given by

$$\tau(R_2) = \int_0^{R_2} \beta_e dR, \quad (12)$$

where β_e is the volume extinction cross section. If there is no absorption $\beta_e = \beta_s$. Finally, $\mathbf{L}(-i_2)$ represents the linear transformation matrix for the scattered light due to the rotation of the coordinate axes (Chandrasekhar, 1950), where i_2 is the angle between the scattering plane OAB and meridian plane OZP_2. The linear transformation matrix is defined by

$$\mathbf{L}(i) = \begin{bmatrix} \cos^2 i & \sin^2 i & \tfrac{1}{2}\sin 2i & 0 \\ \sin^2 i & \cos^2 i & -\tfrac{1}{2}\sin 2i & 0 \\ -\sin 2i & \sin 2i & \cos 2i & 0 \\ 0 & 0 & 0 & 1 \end{bmatrix}. \quad (13)$$

Similarly, the singly scattered light reaching dv_2 can be written as

$$d\mathbf{F}^{(1)} = \frac{\beta_s \mathbf{P}(\theta_1)\mathbf{L}(i_1)\mathbf{F}^{(0)} \exp[-\tau(l_1)]}{4\pi l_1^2} dv_1, \quad (14)$$

where l_1 is the distance between dv_1 and dv_2, and $\mathbf{F}^{(0)}$ represents the flux intensity matrix emitted from the lidar transmitter to the position dv_1 and is given by

$$\mathbf{F}^{(0)} = \begin{bmatrix} F_l^{(0)} \\ F_r^{(0)} \\ U^{(0)} \\ V^{(0)} \end{bmatrix}. \quad (15)$$

Note that $\mathbf{P}(\theta_1)$, $\mathbf{L}(i_1)$, and $\tau(l_1)$ in Eq. (14) have physical meanings similar to those described in Eqs. (10), (13) and (12) and they can be determined using these equations.

Substituting Eq. (14) into (8), we obtain the doubly backscattered light at the point of receiver in the form

$$d\mathbf{F}^{(2)} = \mathbf{f}^{(2)} dv_1 dv_2, \quad (16)$$

where

$$\mathbf{f}^{(2)} = \frac{\beta_s^2 \mathbf{L}(-i_2)\mathbf{P}(\theta_2)\mathbf{P}(\theta_1)\mathbf{L}(i_1)\mathbf{F}^{(0)} \exp[-\tau(l_1) - \tau(R_2)]}{(4\pi)^2 R_2^2 l_1^2}. \quad (17)$$

As mentioned previously, dv_2 denotes the infinitesimal volume confined within two ellipses, which are determined by Eqs. (4) and (6), the field-of-view of the receiver, and the cloud base height. Moreover, the range for dv_1 is confined within the distance R_0 at which single backscattering occurs and the singly scattered light returns to the receiver simultaneously with the doubly backscattered light, the beam width of the transmitter, and the cloud-base height. Thus, carrying out proper integrations we find

$$\mathbf{F}^{(2)} = \iiint_{V_1} \iiint_{V_2} \mathbf{f}^{(2)} dv_1 dv_2$$

$$= \int_0^{2\pi} d\phi_1 \int_0^{\psi_m/2} d\psi_1 \int_{H_b}^{R_0} R_1^2 \sin\psi_1 dR_1 \int_0^{2\pi} d\phi_2 \times \int_0^{\psi_r/2} d\psi_2 \int_{R_{2f}}^{R_{2f'}} \mathbf{f}^{(2)} R_2^2 \sin\psi_2 dR_2, \quad (18)$$

where ψ_m and ψ_r are the beam width of the transmitter and the field-of-view of the receiver, respectively, H_b the cloud-base height, and R_{2f} and $R_{2f'}$ can be determined from Eqs. (4) and (6), respectively. It is clear that the last two parameters must be functions of the five variables $\phi_1, \phi_2, \psi_1, \psi_2$ and R_1.

In addition, equations governing the spherical geometry and angles also are needed in the computation of $\mathbf{F}^{(2)}$. These equations include

$$\cos\theta_1 = \frac{R_2^2 - R_1^2 - l_1^2}{2R_1 l_1}, \quad (19)$$

$$\cos\theta_2 = \frac{R_1^2 - R_2^2 - l_1^2}{2R_2 l_1}, \quad (20)$$

$$\sin i_1 = \frac{\sin\psi_2 \sin(\phi_2 - \phi_1)}{\sin\Delta_{21}}, \quad (21)$$

$$\sin i_2 = \frac{\sin\psi_1 \sin(\phi_2 - \phi_1)}{\sin\Delta_{21}}, \quad (22)$$

$$l_1^2 = R_1^2 + R_2^2 - 2R_1 R_2 \cos\Delta_{21}. \quad (23)$$

Thus, all the physical quantities in Eq. (18) may be expressed in terms of six variables in spherical coordinates. If the polarization characteristics of the incident light are known, then the doubly backscattered flux density may be calculated from Eq. (18).

In this analysis we assume that the transmitted laser light is linearly polarized along the X axis i.e., l direction (see Fig. 1). Under this assumption, the Stokes parameters for the transmitted laser power $\mathbf{P}_t$ may be expressed by

$$\mathbb{P}_t = \begin{bmatrix} P_t \\ 0 \\ 0 \\ 0 \end{bmatrix} = P_t \mathbf{u}, \quad (24)$$

where we let

$$\mathbf{u} = \begin{bmatrix} 1 \\ 0 \\ 0 \\ 0 \end{bmatrix}. \quad (25)$$

Note that $\mathbb{P}_t$ is defined in reference to the Cartesian coordinate system OXYZ. However, $\mathbf{F}^{(0)}$ is expressed on the meridian plane OP_1Z with respect to the spherical polar coordinate system. Thus, we need to apply a linear transformation matrix $\mathbb{L}(-\phi_1)$ to rotate $\mathbb{P}_t$ to the plane OP_1Z. In addition, it is assumed that the transmitted power from the lidar system is evenly distributed within the beam of the transmitter so that $\mathbf{F}^{(0)}$ may be written as

$$\mathbf{F}^{(0)} = \frac{P_t \mathbb{L}(-\phi_1)\mathbf{u} \exp[-\tau(R_1)]}{2\pi R_1^2 [1 - \cos(\psi_m/2)]}. \quad (26)$$

All physical quantities in Eq. (26) have been defined previously. Substituting Eq. (26) into (17) and (18), the doubly backscattered power, $\mathbf{P}_r^{(2)}$, for transmitted light linearly polarized in the X axis may be written in terms of a power transfer function as follows:

$$\mathbf{T}^{(2)} = \frac{\mathbf{P}_r^{(2)}}{P_t} = \int_0^{2\pi} d\phi_1 \int_0^{\psi_m/2} \sin\psi_1 d\psi_1 \times \int_{H_b}^{R_0} dR_1 \int_0^{2\pi} d\phi_2 \int_0^{\psi_r/2} \sin\psi_2 d\psi_2 \int_{R_{2f}}^{R'_{2f}} \mathbf{f}_l^{(2)} dR_2, \quad (27)$$

with

$$\left.\begin{aligned} \mathbf{f}_l^{(2)} &= \frac{A_p \beta_s^2 \mathbf{L}(-\phi_2)\mathbf{M}^{(2)}\mathbf{L}(-\phi_1)\mathbf{u} \exp\{-\tau[2R_0 - H_b(\sec\psi_1 + \sec\psi_2)]\}}{32\pi^3[1 - \cos(\psi_m/2)]l_1^2} \\ \mathbf{M}^{(2)} &= \mathbf{L}(-i_2)\mathbf{P}(\theta_2)\mathbf{P}(\theta_1)\mathbf{L}(i_1) \end{aligned}\right\}, \quad (28)$$

where $\mathbf{P}_r^{(2)}$ represents doubly backscattered power collected by the receiver, A_p the aperture of the receiver, and $\mathbf{L}(-\phi_2)$ the transformation matrix, which rotates the backscattered power matrix to the original Cartesian coordinate system OXYZ, corresponding to the transmitted light.

3. Mathematical formulation for triple backscattering

The procedure for solving the triple backscattering problem follows that for double backscattering. As shown in Fig. 2, let points A, B and C denote, respectively, positions of the infinitesimal volumes dv_1, dv_2 and dv_3 at which first-, second- and third-order scattering occur. The spherical polar coordinate systems for these three scattering events are represented by (ϕ_1, ψ_1, R_1), (ϕ_2, ψ_2, R_2), and (ϕ_3, ψ_3, R_3) where R_1, R_2 and R_3 are the distance between points A, B, and C and point O, respectively. l_1 and l_2 shown in Fig. 2 are distances between A and B and between B and C, respectively. With these definitions, it is evident that the time-dependent triple backscattering must follow the following geometrical relationship

$$2R_0 = R_1 + l_1 + l_2 + R_3. \tag{29}$$

In a manner similar to the double backscattering formulation, the mathematical expression for the triply backscattered flux density due to three infinitesimal volumes may be written as

$$d\mathbf{F}^{(3)} = \mathbf{f}^{(3)} dv_1 dv_2 dv_3, \tag{30}$$

where

$$\mathbf{f}^{(3)} = \frac{\beta_s^3 \mathbf{M}^{(3)} \mathbf{F}^{(0)} \exp[-\tau(l_1) - \tau(l_2) - \tau(R_3)]}{(4\pi)^3 l_1^2 l_2^2 R_3^3}, \tag{31}$$

$$\mathbf{M}^{(3)} = \mathbf{L}(-i_3)\mathbf{P}(\theta_3)\mathbf{P}(\theta_2)\mathbf{L}(i_2)\mathbf{P}(\theta_1)\mathbf{L}(i_1). \tag{31a}$$

In Eq. (31a), $i_2 = i_{21} + i_{23}$; $\mathbf{P}(\theta_1)$, $\mathbf{P}(\theta_2)$ and $\mathbf{P}(\theta_3)$ represent the scattering phase matrices for the three scattering events with θ_1, θ_2 and θ_3 being the scattering angles, $\mathbf{L}(i_1)$, $\mathbf{L}(i_2)$, and $\mathbf{L}(-i_3)$ are linear transformation matrices for the rotation of axes corresponding to the three scattering events, and $\tau(l_1)$, $\tau(l_2)$ and $\tau(R_3)$ are optical depths along the path lengths l_1, l_2 and R_3 (see Fig. 2).

Hence, the triply backscattered flux density matrix may be obtained by performing proper integrations in Eq. (30) as follows:

$$\mathbf{F}^{(3)} = \iiint_{V_1} \iiint_{V_2} \iiint_{V_3} \mathbf{f}^{(3)} dv_1 dv_2 dv_3. \tag{32}$$

The integration range V_1 is the same as that in the double backscattering formulation, while the determination of V_3 is similar to that of V_2 in the double backscattering problem. Note that V_3 is the volume bounded by two ellipses, which have the same foci O and B with different major axes, the field of view of the receiver, and the cloud-base height. The equations of these two ellipses in the spherical polar coordinate system may be written as

$$R_3 = \frac{4a^2 - R_2^2}{4a - 2R_2 \cos\Delta_{32}}, \tag{33}$$

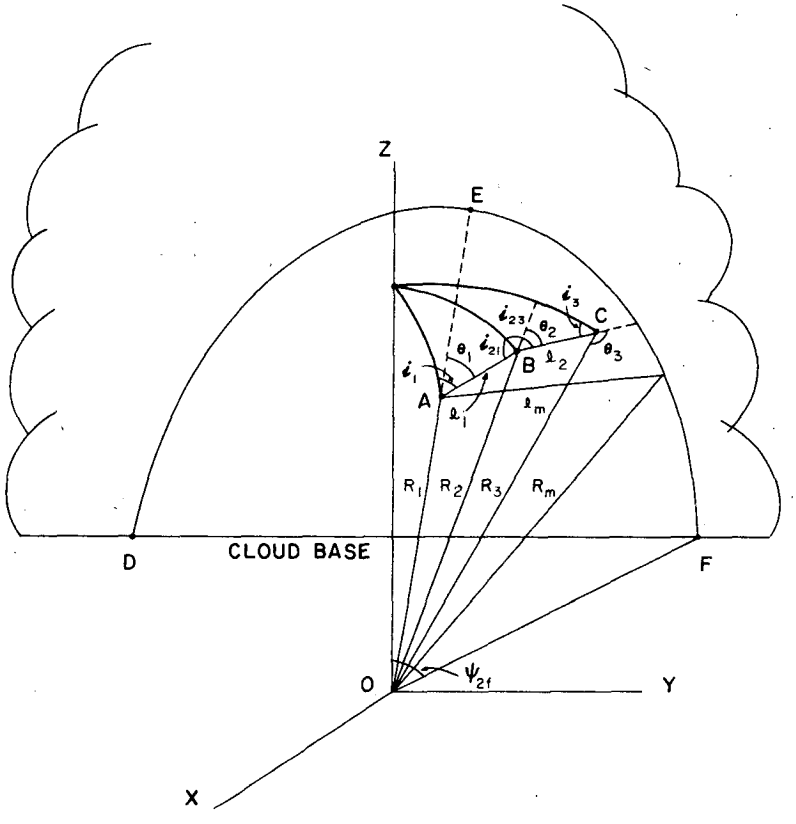

FIG. 2. Geometrical configuration for triple backscattering.

$$R_3' = \frac{4a'^2 - R_2^2}{4a' - 2R_2\cos\Delta_{32}}, \quad (34)$$

where Δ_{32} is the angle between OB and OC, and the major axes of the two ellipses $2a$ and $2a'$ are given by

$$2a = 2R_0 - R_1 - l_1, \quad (35)$$

$$2a' = 2R_0 - R_1 - l_1 + \Delta h. \quad (36)$$

Now we wish to discuss the determination of the integration limit V_2 in Eq. (32). According to Eq. (29) the following relation may be written when R_1 is considered to be a fixed value

$$l_1 + l_2 + R_3 = 2R_0 - R_1 = \text{constant}. \quad (37)$$

Assuming that there is an ellipse which has two foci at points O and A and which satisfies the following equation (see Fig. 2)

$$l_m + R_m = 2R_0 - R_1 = \text{constant}, \quad (38)$$

then, from the geometry it is seen that if secondary scattering takes place outside the aforementioned ellipse (i.e., point B is outside the ellipse) we must have

$$l_1 + l_2 + R_3 > l_m + R_m = 2R_0 - R_1. \quad (39)$$

Consequently, only the points within the ellipse will satisfy the time-dependent relation denoted in Eq. (37). Thus, the integration limit V_2 must be the volume which is confined within the spheroid DEF and above the cloud base. Such a spheroid can be obtained by rotating the ellipse defined in Eq. (38) with respect to the axis OA.

It follows that Eq. (32) may be rewritten in the form

$$\mathbf{F}^{(3)} = \int_0^{2\pi} d\phi_1 \int_0^{\psi_m/2} d\psi_1 \int_{H_b}^{R_0} R_1^2 \sin\psi_1 dR_1 \times \int_0^{2\pi} d\phi_2 \int_0^{\psi_{2f}} d\psi_2 \int_{H_b}^{R_{2f}} R_2^2 \sin\psi_2 dR_2 \times \int_0^{2\pi} d\phi_3 \int_0^{\psi_r/2} d\psi_3 \int_{R_{3f}}^{R'_{3f}} \mathbf{f}^{(3)} R_3^2 \sin\psi_3 dR_3, \quad (40)$$

where the integration limits R_{3f} and R'_{3f} can be determined by the ellipses given by Eqs. (33) and (34), and R_{2f} is defined by the equation of the ellipse which satisfies Eq. (38) and may be written as

$$R_{2f} = \frac{(2R_0 - R_1)^2 - R_1^2}{2(2R_0 - R_1) - 2R_1\cos\Delta_{21}}, \quad (41)$$

where

$$\cos\Delta_{21} = \cos\psi_2\cos\psi_1 + \sin\psi_2\sin\psi_1\cos(\phi_2 - \phi_1). \quad (42)$$

As for ψ_{2f}, on the basis of the geometry shown in Fig. 2 we find

$$\psi_{2f} = \cot^{-1}(A/B) - \cos^{-1}[C(A^2 + B^2)^{-1/2}], \quad (43)$$

where

$$A = (2R_0 - R_1)^2 - R_1^2 + 2R_1H_b\cos\psi_1,$$

$$B = 2R_1H_b\sin\psi_1\cos(\phi_2 - \phi_1),$$

$$C = 4H_b(2R_0 - R_1).$$

In these equations all the notations have been explained in Section 2.

Again, let the transmitted light be linearly polarized in the X axis, then the triply backscattered power may be written in the form

$$\mathbf{T}^{(3)} = \frac{\mathbf{P}_r^{(3)}}{P_t} = \int_0^{2\pi} d\phi_1 \int_0^{\psi_m/2} \sin\psi_1 d\psi_1 \times \int_{H_b}^{R_0} dR_1 \int_0^{2\pi} d\phi_2 \int_0^{\psi_{2f}} \sin\psi_2 d\psi_2 \int_{H_b}^{R_{2f}} R_2^2 dR_2 \times \int_0^{2\pi} d\phi_3 \int_0^{\psi_r/2} \sin\psi_3 d\psi_3 \int_{R_{3f}}^{R'_{3f}} \mathbf{f}_l^{(3)} dR_3, \quad (44)$$

where

$$\mathbf{f}_l^{(3)} = \frac{A_p\beta_s^3\mathbf{L}(-\phi_3)\mathbf{M}^{(3)}\mathbf{L}(-\phi_1)\mathbf{u}}{128\pi^4(1 - \cos\psi_m/2)l_1^2l_2^2} \times \exp\{-\tau[2R_0 - H_b(\sec\psi_1 + \sec\psi_3)]\}. \quad (45)$$

4. General mathematical expression for multiple backscattering

In accord with the formulation of the double and triple backscattering described in Sections 2 and 3, the general mathematical expression for multiple backscattering may be directly written in the form

$$\mathbf{F}^{(n)} = \iiint_{V_1} \iiint_{V_2} \cdots \iiint_{V_n} \mathbf{f}^{(n)} dv_1 dv_2 \cdots dv_n, \quad (46)$$

where

$$\mathbf{f}^{(n)} = \frac{\beta_s^n\mathbf{M}^{(n)}\mathbf{F}^{(0)}}{(4\pi)^n l_1^2 l_2^2 \cdots l_{n-1}^2 R_n^2} \times \exp[-\tau(l_1 + l_2 + \cdots l_{n-1} + R_n)],$$

$$\mathbf{M}^{(n)} = \mathbf{L}(-i_n)\mathbf{P}(\theta_n)\mathbf{P}(\theta_{n-1})\mathbf{L}(i_{n-1})\mathbf{P}(\theta_{n-2})\mathbf{L}(i_{n-2}) \cdots \mathbf{P}(\theta_1)\mathbf{L}(i_1). \quad (47)$$

And the time-dependent relationship in this case is given by

$$2R_0 = R_1 + l_1 + l_2 + \cdots + l_{n-1} + R_n. \quad (48)$$

For all orders of backscattering it is assumed that the first, second, $\cdots$ and nth-order scattering events take place at points A_1, A_2, $\cdots$ A_n, respectively, with differential volumes dv_1, dv_2, $\cdots$ and dv_n. The associated coordinate systems are (ϕ_1, ψ_1, R_1), (ϕ_2, ψ_2, R_2), $\cdots$ and (ϕ_n, ψ_n, R_n). Let θ_1, θ_2, $\cdots$ and θ_n be scattering angles, and i_1, i_2, $\cdots$ and i_n be the angles between the scattering planes in a manner similar to those defined in cases of double and triple

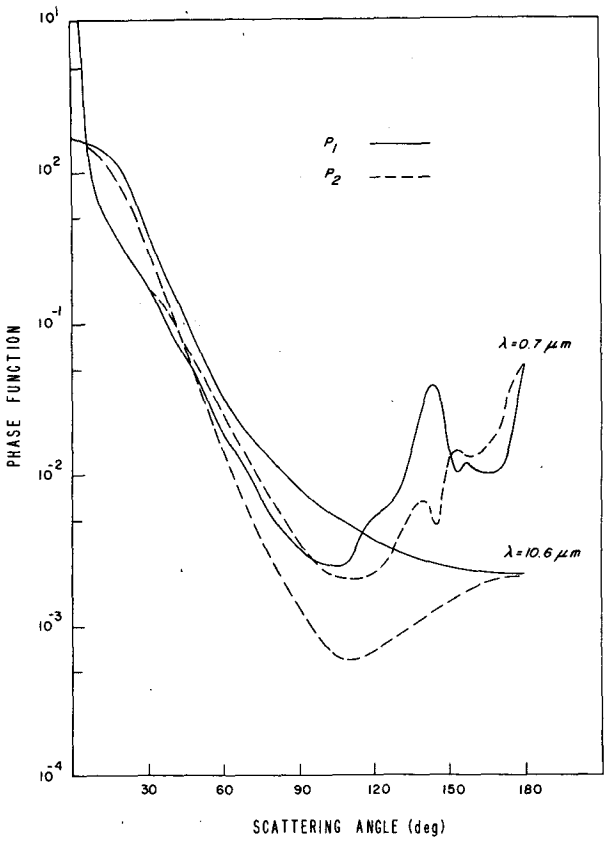

FIG. 3. Scattering phase functions parallel (solid lines) and perpendicular (dotted lines) to the scattering plane of a typical fair weather cumulus cloud for 0.7 and 10.6 μm laser wavelengths.

backscattering. It follows that $\mathbf{P}(\theta_1)$, $\mathbf{P}(\theta_2)$, $\cdots$ and $\mathbf{P}(\theta_n)$ and $\mathbf{L}(i_1)$, $\mathbf{L}(i_2)$, $\cdots$ and $\mathbf{L}(i_n)$ represent the scattering phase matrices and linear transformation matrices, respectively. In addition, l_1, l_2, $\cdots$ and l_{n-1} denote distances between points A_1 and A_2, between A_2 and A_3, $\cdots$ and between A_{n-1} and A_n, respectively.

Having defined these parameters, the integrating range in Eq. (46) can be written as

$$\iiint_{V_1} dv_1 = \int_0^{2\pi} d\phi_1 \int_0^{\psi_m/2} d\psi_1 \int_{H_b}^{R_0} R_1^2 \sin\psi_1 dR_1, \quad (49)$$

$$\iiint_{V_2} dv_2 = \int_0^{2\pi} d\phi_2 \int_0^{\psi_{2f}} d\psi_2 \int_{H_b}^{R_{2f}} R_2^2 \sin\psi_2 dR_2, \quad (50)$$

$$\vdots$$

$$\iiint_{V_{n-1}} dv_{n-1} = \int_0^{2\pi} d\phi_{n-1} \int_0^{\psi_{(n-1)f}} d\psi_{n-1} \times \int_{H_b}^{R_{(n-1)f}} R_{n-1}^2 \sin\psi_{n-1} dR_{n-1}, \quad (51)$$

$$\iiint_{V_n} dv_n = \int_0^{2\pi} d\psi_n \int_0^{\psi_r/2} d\psi_n \int_{R_{nf}}^{R'_{nf}} R_n^2 \sin\psi_n dR_n, \quad (52)$$

where

$$\psi_{(n-1)f} = \cot^{-1}\left(\frac{A_{n-1}}{B_{n-1}}\right) - \cos^{-1}\left[\frac{C_{n-1}}{(A_{n-1}^2 + B_{n-1}^2)^{1/2}}\right],$$

$$A_{n-1} = 4a_{n-1}^2 - R_{n-2}^2 + 2R_{n-2}H_b \cos\psi_{n-2},$$

$$B_{n-1} = 2R_{n-2}H_b \sin\psi_{n-2} \cos(\phi_{n-1} - \phi_{n-2}),$$

$$C_{n-1} = 8a_{n-1}H_b,$$

$$2a_{n-1} = 2R_0 - R_1 - l_1 - l_2 - \cdots - l_{n-2},$$

$$R_{(n-1)f} = \frac{4a_{n-1}^2 - R_{n-2}^2}{4a_{n-1} - 2R_{n-2}\cos\Delta_{n-1,n-2}},$$

$$\cos\Delta_{n-1,n-2} = \cos\psi_{n-1}\cos\psi_{n-2} + \sin\psi_{n-1}\psi_{n-2}\cos(\phi_{n-1} - \phi_{n-2}),$$

$$R_{nf} = \frac{4a_n^2 - R_{n-1}^2}{4a_n - 2R_{n-1}\cos\Delta_{n,n-1}},$$

$$R'_{nf} = \frac{4a_n'^2 - R_{n-1}^2}{4a'_n - 2R_{n-1}\cos\Delta_{n,n-1}},$$

$$2a_n = 2R_0 - R_1 - l_1 - l_2 - \cdots - l_{n-1},$$

$$2a'_n = 2a_n + \Delta h.$$

In principle, computations may be successively carried out for nth-order backscattering using the foregoing equations. Also, it should be noted that the theoretical formulation presented here is general and may be modified and applied to any time-dependent multiple scattering problem involving a specific geometry.

5. Numerical results and discussion

In this study, we have utilized an incident laser beam linearly polarized in the X axis throughout the numerical computations. Other incident polarization characteristics also may be used, however. Clouds are assumed to be composed of spherical particles with a gamma size distribution described by Deirmendjian (1969). The mode radius and concentration for the cloud model are $r_c = 4$ μm and $N = 100$ cm^{-3}, respectively. Such a cloud model resembles a typical cumulus cloud in the atmosphere. Under the assumption of independent scattering, the scattering phase matrix for a sample of randomly located spherical drops is given by

$$\mathbf{P}(\theta) = \begin{bmatrix} P_1 & 0 & 0 & 0 \\ 0 & P_2 & 0 & 0 \\ 0 & 0 & P_3 & P_4 \\ 0 & 0 & -P_4 & P_3 \end{bmatrix}. \quad (53)$$

Shown in Fig. 3 are the normalized phase functions P_1 and P_2 for two laser wavelengths at 0.7 and

10.6 μm obtained from a Mie scattering program. For 0.7 μm, the phase functions are characterized by the sharp diffraction peak and features of rainbows and glory. These features disappear for 10.6 μm owing to large absorption of water drops. Also, the diffraction peak is much reduced. The behavior of P_3 is similar to P_1 and P_2, but P_4 contains negative values. Graphs of P_3 and P_4 are not shown here. Utilizing the numerical values for the volume scattering and extinction cross sections and the phase functions, computations for double and triple backscattering were carried out based on Eqs. (27) and (44).

For comparison purposes, computations also were made for primary backscattering. The first-order transfer equation for incident linearly polarized light is simply given by

$$T_1 = \frac{P_r^{(1)}}{P_t} = \frac{A_p \beta_s \Delta h P_1(\pi)}{8\pi R_0^2} \exp[-2\tau(R_0 - H_b)], \quad (54)$$

where $P_r^{(1)}$ is the primary backscattered power, and $P_1(\pi)$ is the first element of the phase matrix when the scattering angle $\theta = \pi$.

In numerical computations it is assumed that the height of the cloud base $H_b = 1000$ m, the aperture of the receiver $A_p = 0.071$ m^2 which is equivalent to a diameter of 30 cm, and the pulse length $\Delta h = 3$ m. The volume scattering and extinction cross sections for the cumulus cloud model are $\beta_s = \beta_e = 16.73$ km^{-1} for $\lambda = 0.7$ μm, and $\beta_s = 4.52$ km^{-1} and $\beta_e = 9.21$ km^{-1} for $\lambda = 10.6$ μm. The beam width of the transmitter and the field-of-view of the receiver are varied in the calculation so as to investigate their effects on multiple backscattering and polarization characteristics.

Fig. 4 shows results of primary and double backscattering transfer functions as functions of the penetration depth for $\lambda = 0.7$ μm and the transmitter beam width ψ_m and receiver field-of-view ψ_r both of 10^{-2} rad. It is apparent that near the cloud base, the singly backscattered power is much greater than the doubly backscattered power. The sum of the perpendicular and parallel components from doubly backscattered return is an order of magnitude smaller than primary backscattering values within penetration depths of ~30 m. The U and V Stokes components are generally two or three orders of magnitude less than primary backscattering values. The rate of decrease of doubly backscattered returns, however, is far less than that of primary backscattering due to the increasing scattering contribution as the laser beam penetrates through the cloud. When the penetration depth is greater than 300 m, the sum of the doubly scattered power already is larger than the singly scattered power. But the absolute scattered powers for both primary and double backscattering are very small (e.g., $T_{2l} + T_{2r} = 2.5 \times 10^{-15}$ at 300 m).

In carrying out double backscattering computations using Eqs. (17) and (18), there exists the possibility that the integrations become singular, i.e., the scattered fluxes approach infinity, as the distance between two points of scattering, l_1, goes to zero. However, based on both geometrical and physical considerations, when $l_1 \to 0$, $R_1 = R_2 = R_0$ (see Fig. 1), double backscattering is equivalent to primary backscattering. Following this physical principle, a simple computational scheme has been developed to classify cases involving $l_1 = 0$ in primary scattering. It should be pointed out, however, that scattering contributions generated by these cases are insignificantly small (<0.01% of the total).

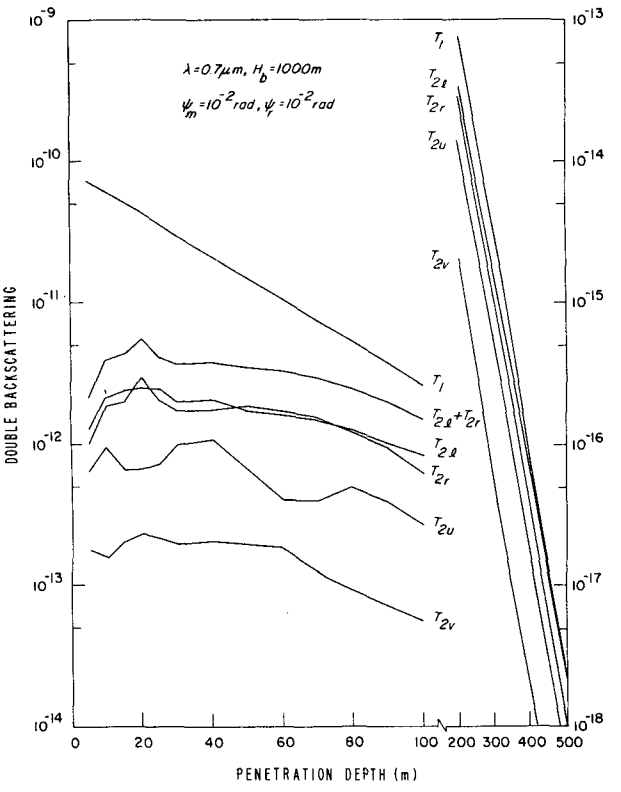

FIG. 4. The singly and doubly backscattered power in terms of the transmitted power defined in Eqs. (54) and (27) as a function of the laser pulse penetration depth for 0.7 μm wavelength using a transmitter beam width and a receiver field-of-view of 10^{-2} rad. T_{2l}, T_{2r}, T_{2u} and T_{2v} correspond to first, second, third and fourth Stokes components, respectively defined in Eq. (9).

In Fig. 5, we study the effect of the transmitter beam width ψ_m on the backscattered power. If ψ_m and ψ_r are both reduced from 10^{-2} to 10^{-3} rad, the doubly backscattered powers from near the cloud base do not change significantly. This is because the intensity of the transmitted laser beam is strengthened within the smaller scattering volume, although the receiver field-of-view is reduced. Only when ψ_r is reduced from 10^{-2} to 10^{-3} rad. does a significant reduction in the doubly backscattered power occur. In this case, double backscattering values are three orders of magnitude smaller than primary backscattering values from returns near the cloud bottom.

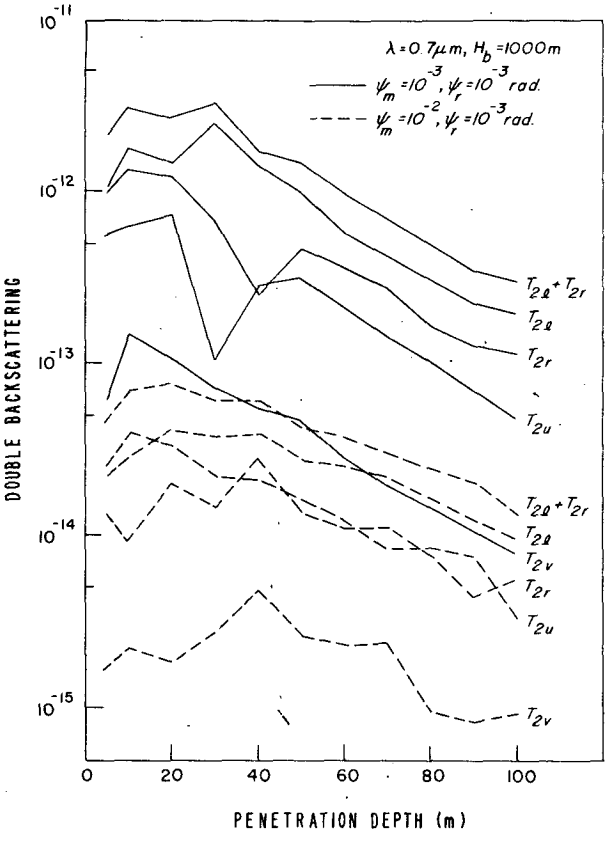

FIG. 5. As in Fig. 4 except using transmitter beam widths of 10^{-2} and 10^{-3} rad and a receiver field-of-view of 10^{-3} rad.

Comparing curves presented in Figs. 4 and 5, we also find that the doubly backscattered power returns decrease more rapidly as the penetration depth increases when the receiver field-of-view is small. In view of these computational results, the effect of the doubly backscattered return is quite significant and should not be ignored for large transmitter beam widths and receiver field of views (say, $\geq 10^{-2}$ rad). Moreover, it also is apparent from these findings that the correct scheme to minimize the double-scattering effect is to utilize a small receiver field-of-view while maintaining a larger transmitter beam width. With these combinations, the primary backscattering remains unchanged, whereas the doubly backscattered power will be greatly reduced.

Fig. 6 illustrates the ratios of doubly to singly backscattered powers as functions of the penetration depth for two sets of ψ_m and ψ_r. When ψ_m and ψ_r both have values of 10^{-2} rad, the ratio is $<10\%$ within the penetration depth of $\sim$20 m. As the penetration depth increases, the ratio increases rapidly. At 100 m, we see a value of 0.56 for $(T_{2l} + T_{2r})/T_1$. But at 500 m, this ratio reaches 1.4. When $\psi_m = \psi_r = 10^{-3}$ rad, the ratios from returns near the cloud base are fairly similar to previous values. But as the penetration depth increases, the rate of increase of the ratio is not as rapid as in the previous case. In the range of 40–100 m, $(T_{2l} + T_{2r})/T_1$ retains a constant value of about 0.1. For penetration depths > 200 m, the doubly backscattered powers are negligibly small and results are not plotted in the figure.

In Figs. 7, 8 and 9, we investigate the relative effect of triple backscattering for ψ_m and ψ_r both having values of 10^{-2} and 10^{-3} rad. In both cases, it is seen that triply backscattered powers are less than $\sim 10^{-13}$ which is about two orders of magnitude smaller than primary backscattering values. The U and V components are even smaller with values $\leq 5 \times 10^{-14}$. In Figs. 7 and 8 we see that the triply backscattered power shows no significant decrease as the penetration depth increases. This is attributed to the fact that the scattering volume, under the time dependent condition, is increasingly available for triple backscattering as the penetration depth increases. In Fig. 9, the value of T_{3l}/T_{2l} even shows increase as a function of the penetration depth. In any event, within the penetration depth of 100 m, the ratio of triply to doubly backscattered power is generally $\leq$10%. Thus, the contribution of the triply backscattered return to the total return is only $<5\%$ and for all practical purposes it may be neglected in the interpretation of lidar backscattering data. Note that it is possible that the triple backscattering contribution could become greater than the double scattering contribution when the receiver field-of-view is larger than the transmitter beam width, because third order scattering may come from volumes outside of the receiver view cone.

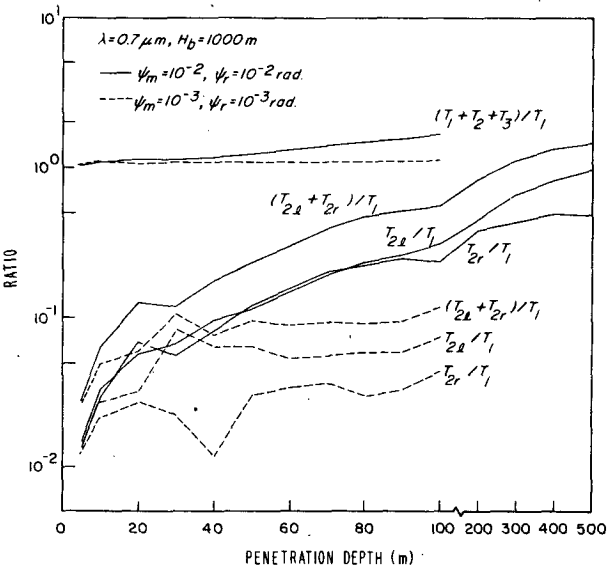

FIG. 6. Ratios of the doubly to singly backscattered power as a function of the laser penetration depth for the perpendicular and parallel components. Also shown are ratios of the total to singly backscattered power.

The total scattered power due to primary, double and triple backscattering is depicted in Fig. 10. Here, we note that $T_2 = T_{2l} + T_{2r}$, and $T_3 = T_{3l} + T_{3r}$, representing the sum of backscattered transfer functions due to parallel and perpendicular components. When ψ_m and $\psi_r = 10^{-2}$ rad, there are appreciable multiple scattering contributions in the lidar backscattering return which remain fairly constant as a function of the penetration depth. In addition, $T_{2r} + T_{3r}$ values will decrease much more slowly than $T_1 + T_{2l} + T_{3l}$ values because T_1 increases drastically near the cloud bottom. We also find from Figs. 4, 5 and 10 that multiply backscattered energy T_{2r} or $T_{2r} + T_{3r}$ has a maximum at the penetration depth of ~20 m. In an earlier paper, Pal and Carswell (1973) reported, based on a number of field polarization observations, that the backscattered return profile for the parallel component (i.e., $T_1 + T_{2l} + T_{3l}$ in our notation) has a narrower peak than that for the perpendicular component (i.e., $T_{2r} + T_{3r}$) and that the peak value of the parallel component occurs ~40 m below that of the perpendicular component for a relatively homogeneous cloud. These results implied, they argued, that the return power of the parallel component would build up much more rapidly than that of the perpendicular component. Our foregoing theoretical results appear to be in harmony with their observational findings and explain the fact

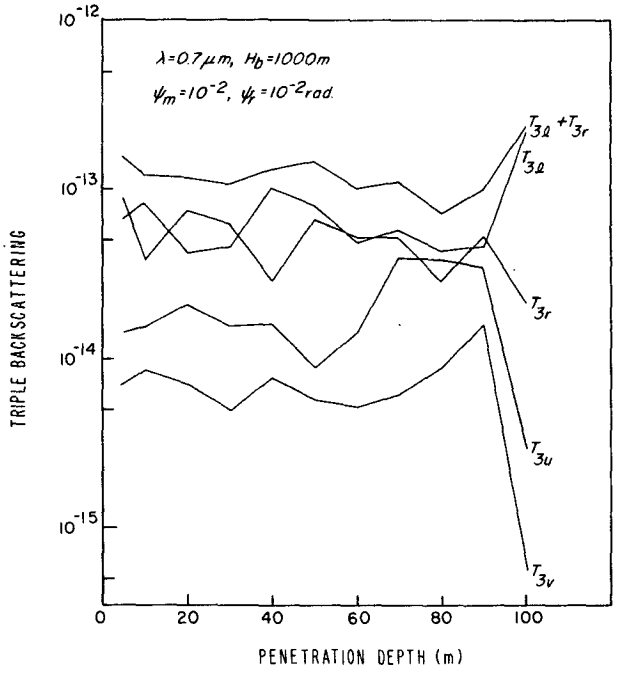

FIG. 7. The triply backscattered power of four Stokes parameters in terms of the transmitted power defined in Eq. (44) as a function of the laser penetration depth for a transmitter beam width and a receiver field-of-view of 10^{-2} rad. T_{3l}, T_{3r}, T_{3u} and T_{3v} correspond to first, second, third and fourth Stokes components defined in Eq. (9).

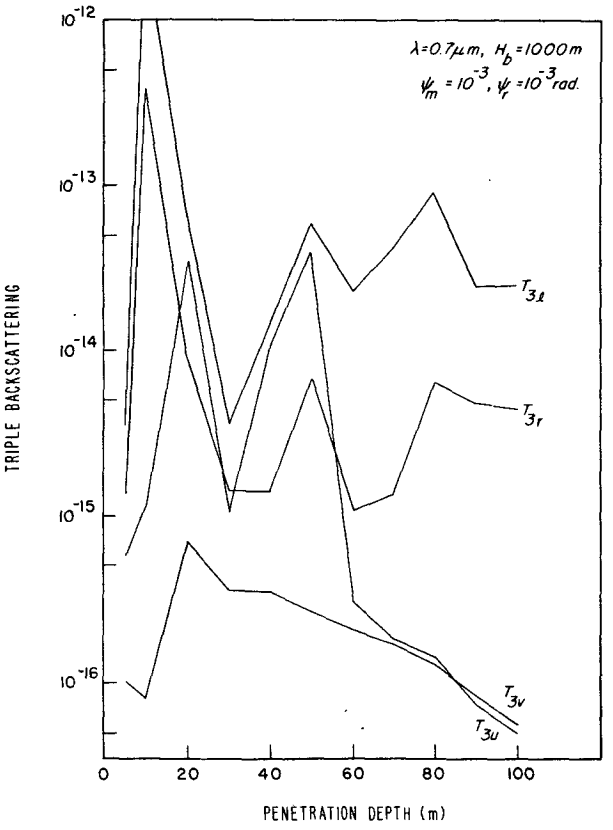

FIG. 8. As in Fig. 7 except for a transmitter beam width and a receiver field-of-view of 10^{-3} rad.

that the parallel component contains return energy from primary backscattering which has its maximum return from the position near the cloud base. For nonhomogeneous clouds, however, Pal and Carswell indicated that the distance between the peaks of parallel and perpendicular components are much reduced. Such a reduction would probably imply the existence of nonspherical particles in the cloud.

Moreover, it is also evident that multiple backscattering, particularly triple backscattering, produces fluctuations as the penetration depth increases, Inspection of Figs. 4, 5, 7 and 8 reveals that fluctuations in the returned energy are especially pronounced for small ψ_m and ψ_r. For example, at a penetration depth of 10 m, the triply backscattered return T_{3l} has a value of 3×10^{-12} which is greater than the double backscattering value (2×10^{-12}) at this penetration depth, and is larger than all the triply backscattered return values at other penetration depths by as much as two orders of magnitude. The other Stokes parameters T_{3r}, T_{3u} and T_{3v} also show appreciable variation.

In order to verify whether these oscillations are physically realistic or produced by errors in the finite numerical integration scheme, we have carried out a number of numerical experiments utilizing a Monte

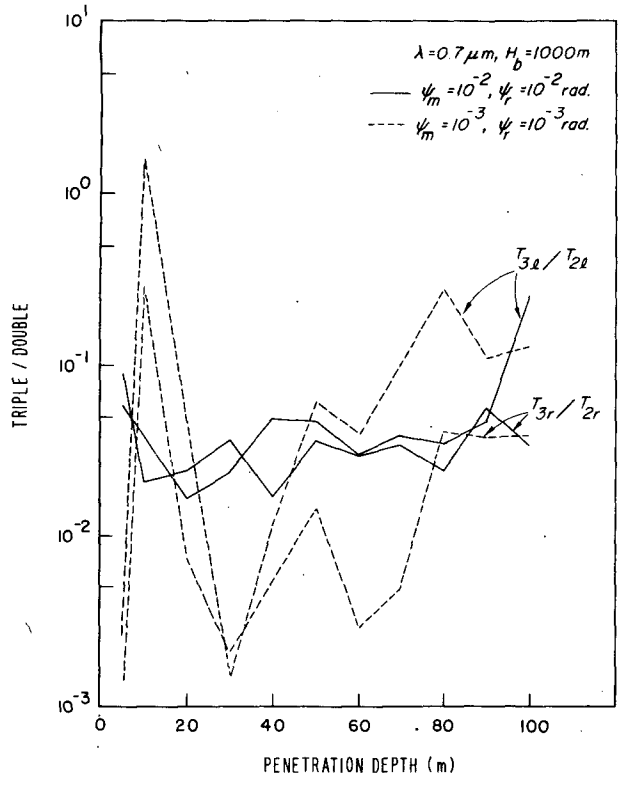

FIG. 9. Ratio of triply to doubly backscattered power as a function of the laser penetration depth.

Carlo integration routine available from the computer center at the University of Utah. This integration subroutine has been found to be the most economic and efficient program in handling high-order integrations. Numerical experiments involving the increase of phase function data and integration points by a factor of two have been performed sequentially. Convergence criterion has been set up such that the results will achieve an accuracy of within 2%. The computer time involved in double scattering computations after convergence has been met is ~6 min. for each penetration depth on the UNIVAC 1108 computer, while for triple scattering it is ~9 min. All of the results presented in Figs. 4–8, based on the aforementioned accuracy, are the real product of backscattering events and are not artifacts of the integration procedure.

These fluctuations are the result of intricate combinations of the available scattering volume, phase function, and exponential attenuation. For double backscattering, we note from Eqs. (17) and (18) that the second order transfer function $T_2 \propto v_1 v_2 P_1(\theta_2) \times P_2(\theta_1) \exp(-2\tau R)$, where v_1 and v_2 are volumes associated with first and second order scattering, respectively. As the laser beam penetrates through the cloud, v_1 and v_2 increase rapidly during which exponential attenuation is still weak. As a result, T_2 increases as the penetration depth increases. But then attenuation becomes increasingly significant and to a certain depth T_2 is bound to be decreasing. Further increase of T_2 is believed to be related to the phase functions. At a wavelength of 0.7 μm, cloud droplets show pronounced rainbow and glory features in the P_1 and P_3 phase matrix components whose values vary by five orders of magnitude. Since there is a requirement for the time-dependent relationship in the computation of multiply backscattered energy for a pulsed lidar system, the returned energy from clouds at a given instant of time is generated from certain scattering angles at which phase functions vary greatly. And the backscattered return energy may show a maximum value by a combination of strong forward scattering and backscattering at the rainbow or glory angle. The larger fluctuations shown in the case of a smaller receiver and transmitter field-of-view (Fig. 5) for T_{2r} and T_{2u} are believed to be associated with the phase function variations. The pronounced and complex oscillations for triple backscattering depicted in Figs. 7 and 8 may be explained by the combined influence of scattering volumes, phase functions, and attenuations. It is not possible, however, to single out a specific cause to account for these large variations in triple backscattering cases. It appears that the effect of multiple scattering is to increase the fluctuation of the backscattered return signal. Thus, when multiple-backscattered signal is measured alone, pronounced

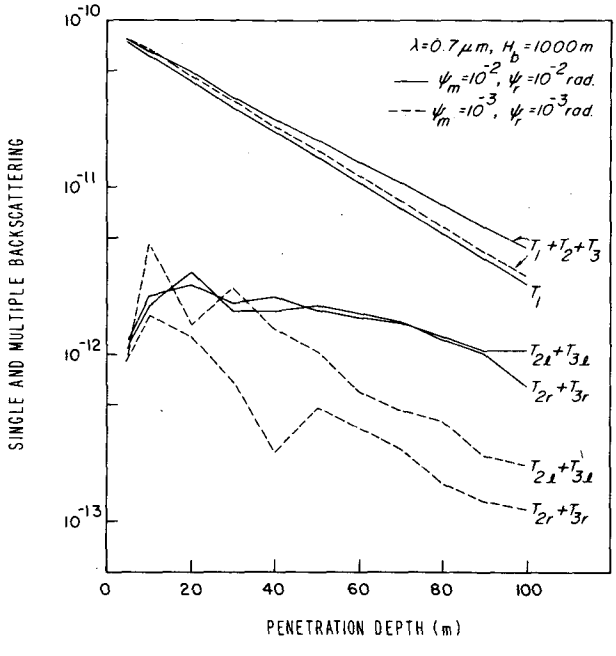

FIG. 10. The sum of doubly and triply backscattered powers in terms of the transmitted power as a function of the laser penetration depth. Also shown are comparisons of the primary and the sum of singly, doubly, and triply backscattered powers.

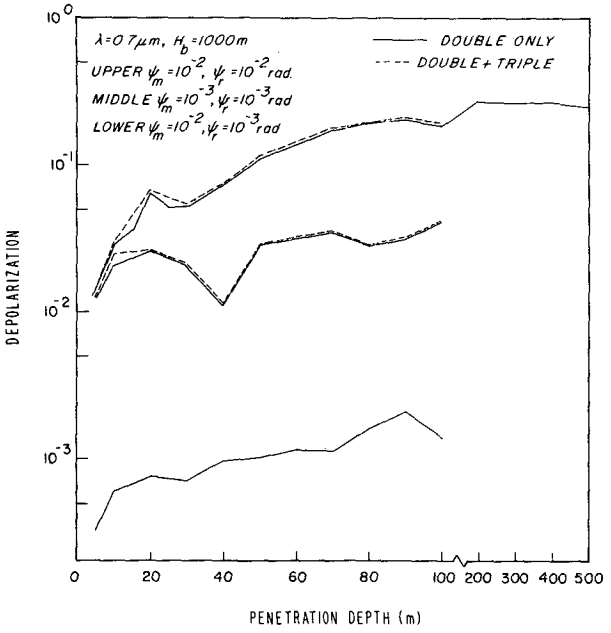

FIG. 11. Depolarization ratios as functions of the laser penetration depth for three sets of values of the transmitter beam width and receiver field-of-view (see text for the definition).

variations as functions of the penetration depth would be anticipated. This theoretical conclusion seems to be in agreement with observations presented and described by Allen and Platt (1977) in their lidar experiment.

In Fig. 11 we examine depolarization ratios due to double $[T_{2r}/(T_1 + T_2)]$ and triple $[(T_{2r} + T_{3r})/(T_1 + T_2 + T_3)]$ backscattering for three different combinations of ψ_m and ψ_r. For ψ_m and $\psi_r = 10^{-2}$ rad, depolarization of the backscattered return increases rather quickly as the laser beam penetrates through the cloud. At ~50 m, depolarization reaches a value of ~10%. At penetration depths $\gtrsim$ 80 m, we see that depolarization ratios remain within ~20–30%. As for $\psi_m = \psi_r = 10^{-3}$ rad, depolarization ratios are generally <5%. We note that there is a minimum depolarization value at a penetration depth of ~40 m which is in accordance with the minimum for T_{2r} (solid line) depicted in Fig. 5. In addition, we also find that depolarization ratios for $\psi_m = 10^{-2}$ rad and $\psi_r = 10^{-3}$ rad are extremely small (<0.2%). The physical reason for insignificant depolarization involving a larger transmitter beam width coupled with a smaller receiver field-of-view is because the transmitted pulsed laser energy spreads into a larger area and only a small portion of the transmitted pulse could return and enter the receiver under the time-dependent constraint. Finally, it is seen that depolarization caused by triple backscattering is normally insignificant and can be neglected for all practical purposes. Thus, for the purpose of reducing the effect of multiple scattering in cloud probing problems, the best approach is to select a small field-of-view for the receiver and maintain a large aperture while enlarging the beam width of the transmitter.

The four Stokes parameters for the backscattered power in terms of the ellipticity, orientation of the elliptically polarized beam, and degree of polarization are illustrated in Figs. 12 and 13. Let $F = F_l + F_r$, and $Q = F_l - F_r$, the ellipticity angle $\beta = \frac{1}{2} \times \sin^{-1}(V/I)$, the orientation angle $\chi = \frac{1}{2} \tan^{-1}(U/Q)$, and the degree of polarization is given by $(Q^2 + U^2 + V^2)^{1/2}/F$. The ellipticity shown in Fig. 12 for the ψ_m and $\psi_r = 10^{-2}$ rad case is very small with a value of ~0.001 rad near the cloud base and it in-

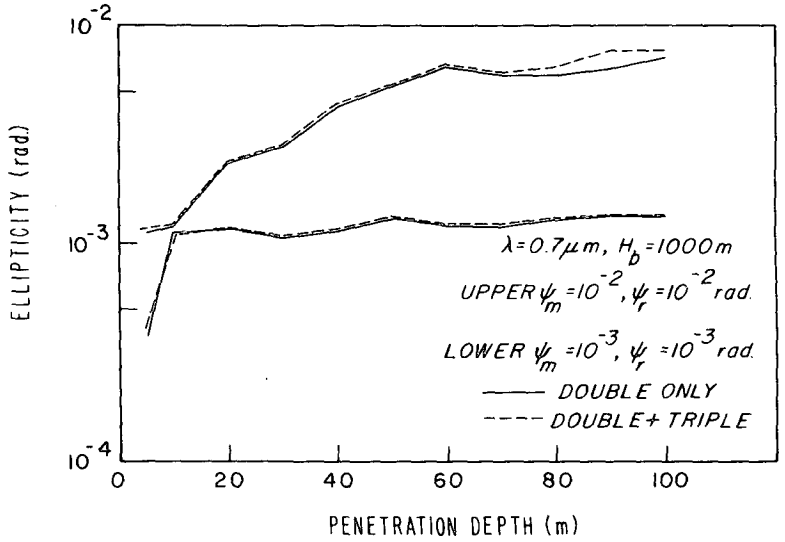

FIG. 12. Ellipticity of the doubly and triply backscattered returns as functions of the laser penetration depth (see text for the definition).

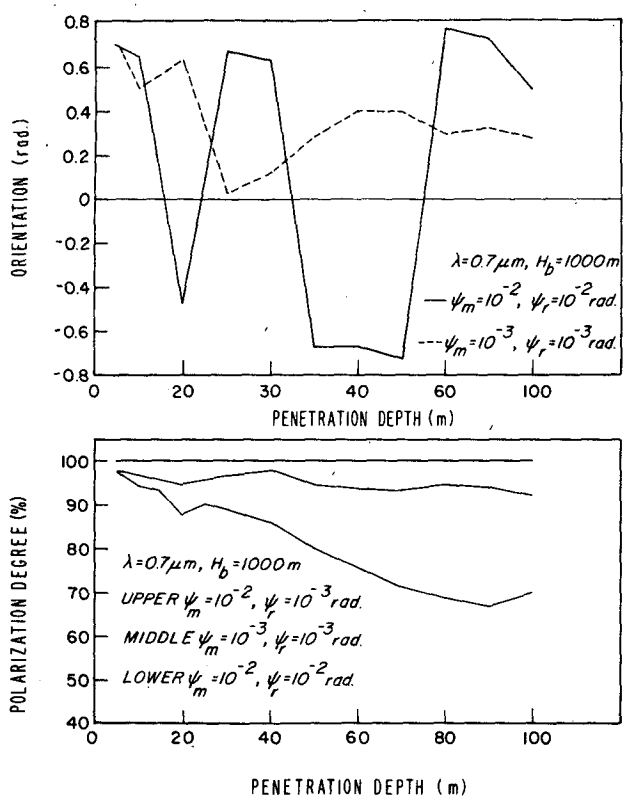

FIG. 13. Orientation angle (upper diagram) and degree of polarization (lower diagram) of the doubly backscattered return as functions of the laser penetration depth (see text for the definition)

creases to ~0.007 rad at 60 m penetration depth. In the case when $\psi_m = \psi_r = 10^{-3}$ rad, the ellipticity beyond the penetration depth of 10 m remains a value within ~0.001–0.002 rad. The backscattered ellipticity for an incident linearly polarized beam is seen to be quite small. Consequently, the return energy has a polarization state very close to linear polarization. At the penetration depth of ~10 m, the backscattered ellipticity for double scattering is slightly larger than that for double plus triple scattering. This may be physically correct since the ellipticity is expressed in terms of angles defined previously. It is also possible that the small differences are caused by computational errors in performing high-order integrations.

The upper diagram in Fig. 13 depicts the orientation of the electric vector for the polarized beam, i.e., the angle between the major axis of the ellipse and the direction of the incident linearly polarized light. When $\psi_m = \psi_r = 10^{-2}$ rad, the orientation angle as a function of the penetration depth fluctuates greatly with values ranging from 0 to ±0.7 rad (±40°). But when $\psi_m = \psi_r = 10^{-3}$ rad, the orientation angle only shows positive values. On the basis of these findings, we may postulate that the physical reason for spherical droplets to generate backscattering depolarization is due to the constant variation of the orientation angle of the electric vector during multiple-scattering processes. In the lower diagram, we show the degree of polarization for the backscattered return. For $\psi_m = \psi_r = 10^{-2}$ rad, its value decreases as the linearly polarized beam penetrates in the cloud. When $\psi_m = 10^{-2}$ rad and $\psi_r = 10^{-3}$ rad, the backscattered return energy essentially retains the polarization state of the incident beam, i.e., there is little depolarization generated in multiple-scattering processes. This conclusion is in agreement with the previous discussion on depolarization. All the above discussions are concerned with a pulsed laser beam having a wavelength of 0.7 μm. Finally, we investigate double backscattering for a pulsed laser beam with a wavelength of 10.6 μm (CO_2 laser). For this wavelength, it is assumed that independent scattering still is valid in clouds so that scattered fluxes may be added without considering the phase of the electric vector. Absorption of water droplets at $\lambda = 10.6$ μm is quite substantial. The single scattering albedo is ~0.49 and the phase function depicted in Fig. 3 shows that rainbow and glory features are suppressed by internal absorption. Fig. 14 displays multiple-backscattered energy curves and shows that values and fluctuations of the backscattered energy are much more reduced as a result of water droplet absorption. The ratio of doubly to singly backscattered powers depicted in Fig. 15 remains fairly constant and has a value of ≤0.5%. Values of triply backscattered return and depolarization both are negligibly small at the 10.6 μm wavelength.

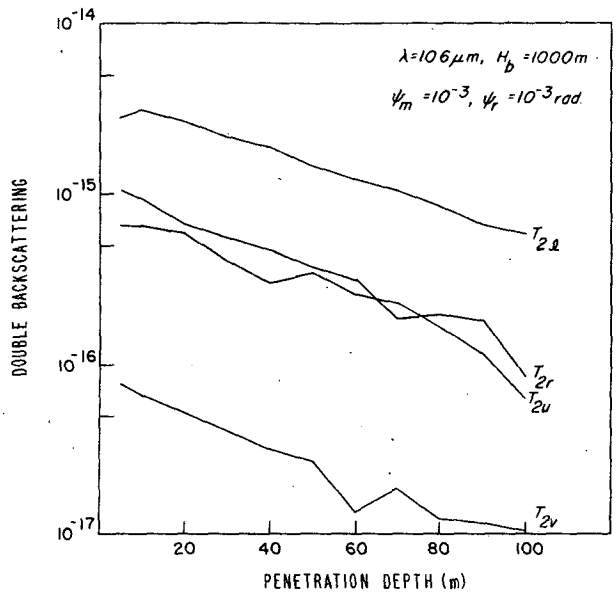

FIG. 14. Doubly backscattered power in terms of the transmitted power for the 10.6 μm wavelength as a function of the laser penetration depth.

6. Conclusion

In this paper, we have developed and derived time-dependent transfer models for double, triple, and general multiple backscattering problems utilizing a spherical polar coordinate system in terms of a series of integral equations. In essence, the theoretical development described in this study is general and no specific physical approximation is required in the mathematical formulation. The time-dependent multiple backscattering model developed in this investigation for the first time includes a general four-by-four scattering phase matrix and is applicable to a colocated transmitter and receiver fixed in a rectangular coordinate system. The present formulation also may be applied to general multiple-scattering problems involving particular geometries.

Numerical computations for doubly and triply backscattered powers have been carried out employing the phase matrix for a cumulus cloud at a visible wavelength to investigate the effects of the transmitter beam width and receiver field-of-view on the backscattered return and polarization characteristics. Relative contribution due to primary, double, and triple backscattering as functions of the penetration depth are examined comprehensively and discussed physically. We also show computational results for an infrared laser wavelength of 10.6 μm at which absorption of water and ice is quite significant. Below we summarize highlights of the computational result and new finds derived from this theoretical analysis.

1) Contributions of multiple backscattering to lidar return energy are significant when the receiver field-of-view and transmitter beam width both have values greater than or equal to 10^{-2} rad. When the laser pulse penetrates beyond ~300 m, we find that the doubly backscattered power can be greater than the singly backscattered power. The double to single backscattering ratio is less than ~0.1 if the receiver field-of-view is limited to be $<10^{-3}$ rad. Therefore, it is recommended that the best approach to minimize the effect of multiple scattering in lidar observations of cloud compositions and structure is to reduce the receiver field-of-view (say to a value of 10^{-3} rad), while a wider transmitter beam width (say a value of 10^{-2} rad) should be adopted at the same time.

2) Backscattered depolarization from a typical cumulus cloud composing exclusively of spherical drops is quite significant with values as large as 20–30% when the transmitter beam width ψ_m and receiver field-of-view ψ_r both have values of 10^{-2} rad. But it is <5% when ψ_m and ψ_r are reduced to 10^{-3} rad. Moreover, depolarization ratios are found to be extremely small with values less than 0.2% for a larger transmitter beam width (10^{-2} rad) coupled with a smaller receiver field-of-view (10^{-3} rad). This is owing to the fact that the transmitted pulsed laser energy spreads into a larger volume but only a small portion could return and enter the receiver field-of-view because of the time-dependent restriction.

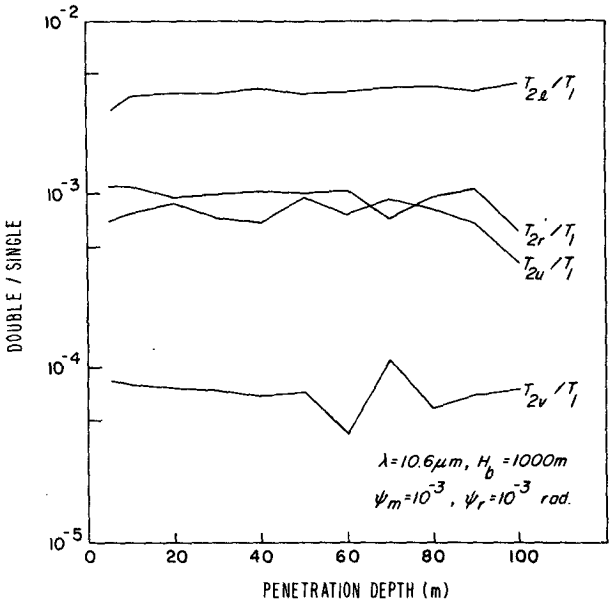

FIG. 15. Ratio of doubly to singly backscattered power for the 10.6 μm wavelength as a function of the laser penetration depth.

3) Multiple backscattering tends to intensify fluctuations of the return power as the penetration depth increases, caused by the coupling of diffraction and scattering at rainbow and glory angles. The present theoretical finding is in agreement with lidar observational results presented and discussed by Allen and Platt (1977). Moreover, the present computational results reveal that the parallel component of the backscattered return has a relatively narrow maximum value from return near the cloud base, whereas the maximum return for the perpendicular component is ~20–40 m above the cloud base. This finding confirms the polarization observations reported by Pal and Carswell (1973) for homogeneous water clouds.

4) The ellipticity of the backscattered energy from water clouds for an incident linearly polarized laser beam at the 0.7 μm wavelength is extremely small. This implies that the backscattered polarization also is nearly linear, but with an orientation differs from the incident linear polarization. However, the orientation of the electric vector varies significantly and constantly as a function of the penetration depth. The constant variation of the orientation angle during multiple scattering processes is precisely the fundamental reason which causes depolarization.

5) Finally, double backscattering and depolarization from water clouds are shown to be insignificant for the 10.6 μm laser beam. A proper selection of

laser wavelengths in the infrared could add a new dimension for cloud sounding when it is coupled with a polarized laser in the visible and near infrared region.

Acknowledgments. This research was supported in part by the Atmospheric Research Section of the National Science Foundation under Grant ATM78-26259 and by the Air Force Office of Scientific Research under Contract F49620-79-C-0198.

REFERENCES

Allen, R. J., and M. R. Platt, 1977: Lidar for multiple backscattering and depolarization observations. *Appl. Opt.*, **16**, 3193–3199.

Chandrasekhar, S., 1950: *Radiative Transfer*. Dover, 393 pp.

Deirmendjian, D., 1969: *Electromagnetic Scattering on Spherical Polydispersions*. Elsevier, 290 pp.

Houston, J. D., and A. I. Carswell, 1978: Four-component polarization measurements of lidar atmospheric scattering. *Appl. Opt.*, **17**, 614–620.

Liou, K. N., 1971: Time-dependent multiple backscattering. *J. Atmos. Sci.*, **28**, 824–827.

——, and R. M. Schotland, 1971: Multiple backscattering and depolarization from water clouds for a pulsed lidar system. *J. Atmos. Sci.*, **28**, 772–784.

Pal, S. R., and A. I. Carswell, 1973: Polarization properties of lidar backscattering from clouds. *Appl. Opt.*, **12**, 1530–1535.

Sassen, K., and K. N. Liou, 1979a: Scattering of polarized laser light by water droplet, mixed phase and ice crystal clouds. Part I. Angular scattering patterns. *J. Atmos. Sci.*, **36**, 838–851.

——, 1979b: Scattering of polarized laser light by water droplet, mixed-phase and ice crystal clouds. Part II. Angular depolarizing and multiple-scattering behavior. *J. Atmos. Sci.*, **36**, 852–861.

Weinman, J. A., 1976: Effect of multiple scattering on light pulses reflected by turbid atmospheres. *J. Atmos. Sci.*, **33**, 1763–1771.